On-line Detection of Imperfections in Laser-brazed Joints

Daniel Fecker, Volker Maergner and Tim Fingscheidt
Institute for Communications Technology
Technical University Braunschweig
Schleinitzstr.22, 38106 Braunschweig, Germany
E-mail: {fecker, maergner, fingscheidt}@ifn.ing.tu-bs.de

Abstract

This paper presents a joint imperfection detection method for on-line process monitoring of laser brazing processes. The method uses images from two spectral ranges and fuses their features with the scores of the separately calculated log-likelihood ratios to decide whether the currently generated part of a joint contains an imperfection or not. To avoid unconfident classifications, a decision reject is implemented. Furthermore, the classifier can be adapted to different quality requirements.

1 Introduction

Laser brazing is a well established joining process in the automotive industry. Especially in visible regions of a vehicle, such as the boot lid, the quality requirements for the brazed joints are very high. Conventionally the quality of a joint is inspected in several test stations after the brazing process. Recently, there have been attempts to combine all testing stations in one system which allows to measure the quality during the brazing process [1–4]. This principle of on-line quality control monitoring is already known from the application of laser welding where several approaches already exist [5, 6].

This paper focuses on the on-line detection of imperfections of the categories pores, joint interrupts and wetting failures. These are the most critical imperfections and are not only affecting the appearance of the joint but also influencing the quality characteristics such as stability and leak tightness of the joint significantly.

The following section gives a quick overview over the experimental setup used for the on-line monitoring of laser brazing. Section 3 describes the feature extraction method which is used by the classifier presented in Section 4. Achieved results are discussed in Section 5, and we give conclusions in Section 6.

2 Experimental Setup

The experimental setup is shown in Figure 1. Two cameras are integrated coaxially in the laserbeam path of a laser optic. The cameras provide synchronous images in two spectral ranges: visual (VIS) and near-infrared (NIR). They allow a detailed observation of the process with up to 300 frames/s per camera with a resolution of 1024×440 pixels (8 bit) in the VIS and 320×148 pixels (14 bit) in the NIR image. The optical setup gives a process resolution of about 8 μm/pixel in the VIS and 26 μm /pixel in the NIR image. Figure 2 shows an example of the images from these two cameras. This figure also shows a picture of a resulting joint with an imperfection in the upper part, a small hole in the joint (pore). A more detailed description of this monitoring system is presented in [1].

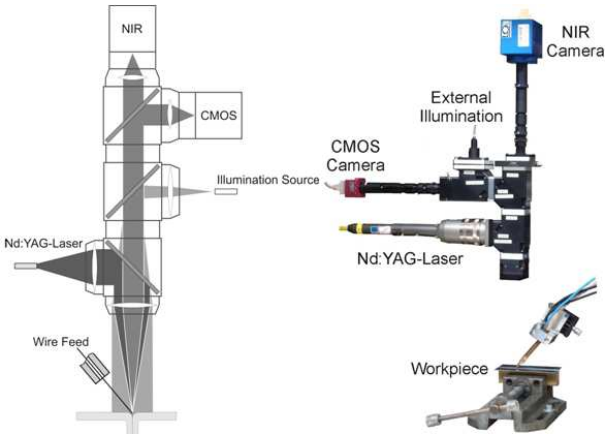

Figure 1. Experimental setup of the monitoring system [2]. For the VIS range a CMOS camera is used. Schematic design (left), realized system (right).

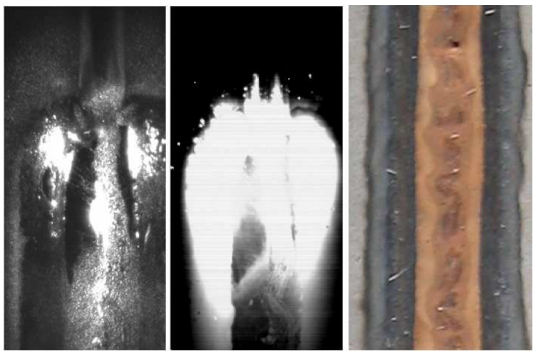

Figure 2. Brazing process in VIS image (left) and NIR image (middle). Processed joint containing a pore (right).

3 Feature Extraction

Due to the high framerate of the cameras, the images captured are highly overlapping. In fact, with a brazing velocity set to 1.3 m/min, new sections of the generated joint appear with a size of about 9 lines in the next VIS and 3 lines in the next NIR image. These sections are inspected a fixed time after the brazing process which allows to monitor fluctuations of the inner heat emissions using the NIR camera. The position of the image section used for inspection is fixed and lo-

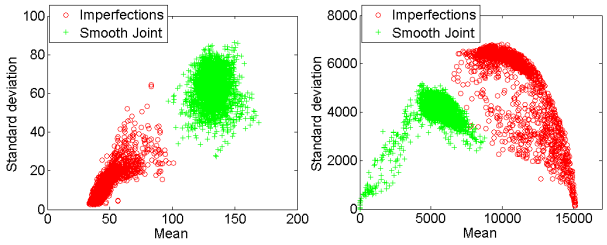

Figure 3. Example of the feature distribution of the different classes from the VIS image (left) and the NIR image (right).

cated directly behind the position of the laser beam. The position of the section in the VIS image is the same in the NIR image. Advantages of this approch are:

- No parts of the joint are missed.
- Small imperfections can be detected.
- Feature extraction is computational inexpensive due to the small amount of pixels in the sections.

Here, we use the global mean and standard deviation of the pixel values in the sections from both images as features. Figure 3 shows an example for the distribution of these $d = 2$ dimensional feature vectors for the class of sections containing imperfections and the one containing a smooth joint surface. It appears that the distribution of the features from the VIS images is much clearer separated and that they may be sufficient for a classification. However, there are cases where samples of one class which are close to the other class in the VIS distribution are more apart in the NIR distribution, and vice versa. To benefit from this effect, the classifier presented in the following section fuses calculated scores of log-likelihood ratios for each sensor individually. To keep it more general, we consider that $\mathbf{X} = (\mathbf{x}_1, \mathbf{x}_2, ..., \mathbf{x}_m, ..., \mathbf{x}_M)$ is a supervector of feature vectors $\mathbf{x}_m$ from each of M sensors (in our case $M = 2$) and that $\mathbf{x}$ denotes any feature vector of this supervector.

4 Classification

The proposed method decides whether $\mathbf{x}$ belongs to one or the other of the following two classes: C_0 represent the class of smooth joint sections without imperfections and C_1 is the class of joint sections with imperfections. Let $D(\mathbf{x}) = i$ imply the decision for choosing C_i, $i = 0, 1$. The Bayes decision rule for this two-category classification states [7]:

$$D(\mathbf{x}) = 0, \text{ if } \frac{p(\mathbf{x}|C_0)}{p(\mathbf{x}|C_1)} > \frac{\lambda_{01} - \lambda_{11}}{\lambda_{10} - \lambda_{00}} \cdot \frac{P(C_1)}{P(C_0)} \quad (1)$$

where $p(\mathbf{x}|C_i)$, $i = 0, 1$ are likelihood functions, $\lambda_{ij} = \lambda(D(\mathbf{x}) = i|C_j)$, $i, j = 0, 1$, is the loss associated with deciding for C_i if the true state of nature is C_j, and $P(C_i)$, $i = 0, 1$, are the *a priori* probabilities for each class. To benefit from the advantages of the logarithm of the likelihood ratio, the condition in (1) can be rewritten as [8]:

$$\log \frac{p(\mathbf{x}|C_0)}{p(\mathbf{x}|C_1)} > \log \frac{\lambda_{01} - \lambda_{11}}{\lambda_{10} - \lambda_{00}} + \log \frac{P(C_1)}{P(C_0)} \quad (2)$$

For a more convenient notation, we substitute

$$L(\mathbf{x}) = \log \frac{p(\mathbf{x}|C_0)}{p(\mathbf{x}|C_1)} \quad (3)$$

and

$$\Lambda' = \log \frac{\lambda_{01} - \lambda_{11}}{\lambda_{10} - \lambda_{00}} \quad (4)$$

where $L(\mathbf{x})$ denotes the log-likelihood ratio and Λ' the loss ratio. The ratio of the *a priori* probabilities $P(C_i)$ and the loss ratio Λ' can be written as $\Lambda = \Lambda' + \log \frac{P(C_1)}{P(C_0)}$, commonly reflecting both entities. Accordingly, we achieve

$$D(\mathbf{x}) = 0, \text{ if } L(\mathbf{x}) > \Lambda. \quad (5)$$

In the case of M sensors with different feature vectors fulfilling the necessary condition of statistical independency, the scores of the log-likelihood ratios can be fused by

$$\hat{L}(\mathbf{X}) = \sum_{m=1}^{M} L(\mathbf{x}_m). \quad (6)$$

This approach benefits from the fact that a currently low score ($L(\mathbf{x}) \approx 0$) of one sensor can be compensated by a higher score of another. Due to the noise of the feature vectors, the Bayes decision (1) is not in all cases the best decision. Especially for $\hat{L}(\mathbf{X}) \approx 0$, a confident decision about the class membership cannot be made. For this reason a threshold variable Δ is introduced which yields the margin $[\Lambda - \Delta; \Lambda + \Delta]$ specifying a state where the class membership is indefinite which infers that a decision is rejected. The value of Δ depends on the kind of the process and has to be chosen dependent on the quality target. If Δ is large, e.g., more test sections are rejected and only high quality joint sections are classified as smooth joint sections. This may make sense if the testing task is crucial. Finally, all previous steps result in the following decision rule:

$$\hat{D}(\mathbf{X}) = \begin{cases} 0 & \text{if } \hat{L}(\mathbf{X}) > \Lambda + \Delta \\ 1 & \text{if } \hat{L}(\mathbf{X}) < \Lambda - \Delta \\ \text{indefinite} & \text{otherwise} \end{cases} \quad (7)$$

Regarding the evaluation of the classifier, the introduction of the indefinite state leads to six classification cases (Table 1). The number of type 1 (T1) errors which are occuring in an evaluation set leads to the *false reject rate* (FRR) and the number of type 2 (T2) errors to the *false accept rate* (FAR).

Besides the introduction of the indefinite state by Δ, we have a second parameter Λ which influences the classification results. Sometimes it is more costly to have more T2 errors than T1 errors or vice versa. Thus, we can apply different values for λ_{ij} in (4) which adjust the ratio of the FAR and FRR. In a non-visible joint,

Table 1. Possible classification cases including a reject decision.

Classified as	Smooth Joint	Imperfection
Smooth Joint	true positive	false positve (type 1 error)
Reject	indefinite (type 2)	indefinite (type 1)
Imperfection	false negative (type 2 error)	true negative

e.g., small imperfections may be allowed to reduce the workpiece scrap rate.

For each sensor and each class the likelihood functions are approximated by density distributions of the training data set. As density distribution functions Gaussian mixture models (GMM) are used because of their ability to approximate arbitrary functions [9]. Since we have multidimensional feature vectors, the mixtures consist of multivariate Gaussian distributions in the form:

$$\mathcal{N}(\mathbf{x};\boldsymbol{\mu},\boldsymbol{\Sigma}) = \frac{1}{(2\pi)^{\frac{d}{2}}|\boldsymbol{\Sigma}|^{\frac{1}{2}}} e^{-\frac{d}{2}(\mathbf{x}-\boldsymbol{\mu})^{\mathrm{T}}\boldsymbol{\Sigma}^{-1}(\mathbf{x}-\boldsymbol{\mu})} \quad (8)$$

where $\boldsymbol{\mu}$ is a d-dimensional mean vector, $\boldsymbol{\Sigma}$ is a $d \times d$ covariance matrix and $|\boldsymbol{\Sigma}|$ is the determinant of $\boldsymbol{\Sigma}$. The GMMs are generated by supervised training using the expectation maximization (EM) algorithm which yields for each class C_i a likelihood function with variable $\mathbf{x}$:

$$p(\mathbf{x}|C_i) = \sum_{k=1}^{K} \omega_{i,k} \cdot \mathcal{N}(\mathbf{x};\boldsymbol{\mu}_{i,k},\boldsymbol{\Sigma}_{i,k}) \quad (9)$$

with K being the number of assumed Gaussian distributions and ω being a weighting factor. Experimental results showed that $K = 4$ Gaussians in a GMM worked well and are used in the following experiments.

5 Experimental Results

The proposed method is tested with the presented monitoring system in a laboratory assembly. Workpiece test pattern joints are brazed having a length of about 15 cm with a flanged geometry. For creating the joint imperfections, the process parameters were adapted to unusual settings. For example, the brazing wire feed rate is lowered in combination with a small lifting of the process head. Thus, imperfections like pores and wetting failures can be generated artificially. Because of the unusual process parameter settings, the overall process often gets unstable and even parts of the joint without imperfections do not have the same quality as a joint generated by stable process conditions.

Our training and evaluation set consists of 25 captured video sequences with imperfections. One of them is a fine specimen with a completely smooth joint and the others are all containing imperfections. The sections of the defective joints having the same smooth appearance as the fine specimen and the sections containing imperfections were annotated to class C_0 and C_1, respectively. The video sequences are further separated in a training (6 sequences) and an evaluation set (19 sequences). Table 2 shows the distribution of the different imperfection types in these sets.

Table 2. Number of imperfections and sections of smooth joints in the training and evaluation set.

	Training	Evaluation
Big Pores	38	55
Medium Pores	54	101
Small Pores	22	92
Wetting Failures	17	48
All Imperfections	131	256
Imperfect Sections	2475	5465
Smooth Sections	2955	7658

Table 3. Classification results for smooth joint sections. $\Lambda = 0$, $\Delta = 0.5$

Features	Smooth Joint	Reject (T2 indef.)	Imperfection (T2 error)
VIS	7657	1	0
NIR	7517	136	5
COMB	7658	0	0

For evaluation of the smooth joint sections, the direct number of classified sections is used. In contrast an imperfection is already regarded as detected if one section containing the imperfection is correctly classified. As results we show absolute values because, due to the general high quality requirements for the brazed joints and the limited amount of data, expressing them in terms of FRR and FAR is not useful. We used $\Lambda = 0$ and $\Delta = 0.5$ in our experiments which corresponds to equal *a priori* probabilities $P(C_0) = P(C_1) = 0.5$ and losses $\lambda_{01} = \lambda_{10} = 1$, $\lambda_{00} = \lambda_{11} = 0$, meaning that T1 and T2 errors are equally costly. In a real, well adjusted process environment $\Lambda = 0$ may also be adequate, since the probability of an imperfection is very low and the cost for a missed imperfection is very high.

Achieved results for the smooth joint sections are listed in Table 3. Indeed, they show that the features from the VIS images are better than those from the NIR images, but the combination (COMB) of both leads to a perfect classification result on this evaluation set.

Table 4 shows results for the evaluation of imperfections. Similar to the evaluation results of smooth joint sections, the VIS features achieving a better detection result than the NIR features. Furthermore, at first glance it looks like the combination of both do not yield a better result. But a closer examination of the missed imperfections reveals that the imperfection types are not the same. Both of the missed imperfections in the VIS images are of the category medium sized pores. They show an unusual appearance: beside the pores are two bright spots with high intensity values. They are affecting the extracted features in such a way that the imperfections are not detected. Otherwise, they are successfully detected in the NIR images which also leads to a successful detection by the combination of both, VIS and NIR. In contrast, the missed and indefinite imperfections of the COMB

Table 4. Imperfection classification results for each sensor and both combined. $\Lambda = 0$, $\Delta = 0.5$

Features	Smooth Joint (T1 error)	Reject (T1 indef.)	Imperfection
VIS	2	1	253
NIR	14	3	239
COMB	2	1	253

Table 5. Imperfection classification results for the combination of both sensors with a variation of Λ. $\Delta = 0.5$

Λ	T2 error	T2 indef.	T1 indef.	T1 error
0	0	0	1	2
2.7	3	5	0	0
-2.7	0	0	3	8

features are very small pores. They are close to the resolution limit and can hardly be detected in the images even by the human eye. It is not mandatory to detect them because they can be overcoated without quality loss.

Table 5 shows achieved detection results for different values of Λ. There are two assumed cases in applications of car body manufacturing:

- Case 1: Visible joint. The quality of the joint surface is crucial. Every error should be detected (increase Λ to minimize amount of T1 errors).
- Case 2: Non-visible joint. Very small imperfections can be missed in order to keep production costs low (decrease Λ to minimize amount of T2 errors).

In case 1 all imperfections are detected at the cost of a few misclassified and rejected smooth sections. In case 2 some imperfections, all of them very small pores, are not detected for allowing a lower quality of classified smooth sections.

For the visualization of the results, the classified joint sections from both cameras are put together to two single mosaic images showing each the whole joint in the VIS and NIR spectral range. The classification result is marked by colors (green = smooth, yellow = reject, red = imperfection) on each side of these mosaics (see Figure 4).

The evaluated method is not only showing good results, also it is pretty fast. The current MATLAB implementation computes 160 frames/s for each camera on an Intel Core i7 920 operating at 2.66 GHz.

6 Conclusions

In this paper we have presented a method for on-line detection of joint imperfections by a classifier based on the fusion of likelihood scores of feature vectors from different sensors. We have shown that the method is adaptable to different process requirements. The number of misclassifications can be reduced by a decision reject based on a classification confidence value. The first evaluation of this method demonstrates promising results and future work will focus on tests in a real process environment.

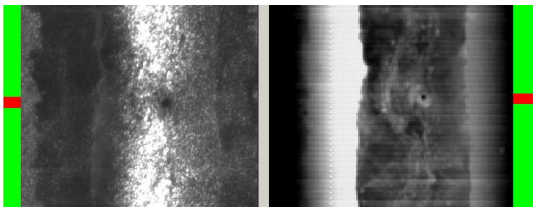

Figure 4. An example of the generated mosaic images with a detected imperfection (marked at both sides).

7 Acknowledgments

The German Federal Ministry of Economics and Technology (BMWI, Project: IN7023-EQOS) is gratefully acknowledged for financial support.

Furthermore, we want to thank our reseach colleagues at Fraunhofer Institute for Production Technology IPT and Fraunhofer Institute for Laser Technology ILT, both in Aachen, Germany, for providing the data.

References

[1] Donst, D., Abels, P., Ungers, M., Klocke, F. and Kaierle, S.: "On-line quality control system for laser brazing," *ICALEO 2009, Proc. 28th Int. Congr. on Applications of Laser & Electro Optics*, Orlando, FL, USA, 2009.

[2] Ungers M., Fecker, D., Frank, S., Donst, D., Maergner, V., Abels, P. and Kaierle, S.: "In-situ quality monitoring during laser brazing," *Physics Procedia: Laser Assisted Net Shape Engineering 6, Proc. of the LANE 2010*, vol.5, no.2, pp.493-503, Erlangen, Germany, 2010.

[3] Kaierle, S., Ungers, M., Franz, C., Mann, S. and Abels, P.: "Understanding the Laser Process," *Laser Technik Journal*, vol.7, no.7, pp.49-52, 2010.

[4] Grimm, A. and Schmidt, M.: "Possibilities for Online Process Monitoring at Laser Brazing Based on Two Dimensional Detector Systems," *ICALEO 2009, Proc. 28th Int. Congr. on Applications of Laser & Electro Optics*, Orlando, FL, USA, 2009.

[5] Shao, J. and Yan, Y.: "Review of Techniques for On-line Monitoring and Inspection of Laser Welding," *Journal of Physics: Conference Series*, vol.15, no.1, pp.101-107, 1995.

[6] Sahli, S., Fissette, S. and Maldague, X.: "Infrared Image Processing for Online Quality Control in Laser Welding," *10th International Conference on Quantitative InfraRed Thermography*, Québec, Canada, 2010.

[7] Duda, R., Hart, P. and Stork, D.: "Pattern Classification, 2. Edition," *Wiley-Interscience*, 2001.

[8] Schum, D. and Pfeiffer, P.: "A Likelihood Ratio Approach to Classification Problems using Discrete Data," *Organizational Behavior and Human Performance*, vol.19, pp.207-225, 1977.

[9] Bishop, C.: "Pattern Recognition and Machine Learning," *Springer (Inf. Science and Statistics)*, 2006.